J. Comp. App. Res. Mech. Eng. Vol. X. No. X, pp. X-X, XXXX *DOI: 10.22061/jcarme.XXXX.XXXX.XXXX*

Journal of Computational and Applied Research in Mechanical Engineering
jcarme.sru.ac.ir
SRTTU
JCARME
ISSN: 2228-7922

Research paper

Time-frequency analysis of vibration signals for bearing fault diagnosis via CWT and t-SNE

Fares Sadji*, Rachid Noureddine and Reda Yahiaoui

Laboratory of Industrial Production and Maintenance Engineering, Institute of Maintenance and Industrial Safety, University of Oran 2 Mohamed Ben Ahmed, Oran, 31000, Algeria.

Article info:

Article history:

Received: 00/00/0000
Revised: 00/00/0018
Accepted: 00/00/0000
Online: 00/00/0000

Keywords:

Bearing fault diagnosis,
Vibration analysis,
Signal processing,
Dimensionality reduction,
CWT,
t-SNE.

***Corresponding author:**
sadji.fares@univ-oran2.dz

Abstract

This study investigates signal processing techniques affect bearing fault diagnosis by analyzing their interaction with feature extraction, dimensionality reduction, and classification. Experiments are conducted on a bearing dataset using raw signals and preprocessed signals based on Fast Kurtogram (FK), Short-Time Fourier Transform (STFT), and Continuous Wavelet Transform (CWT). Support Vector Machine (SVM) and K-Nearest Neighbors (KNN) are used for classification to ensure a fair evaluation with simple models. Furthermore, the time-frequency representations generated by STFT and CWT are processed directly using t-distributed Stochastic Neighbor Embedding (t-SNE). The results show that raw signals provide strong baseline performance, while inappropriate preprocessing may degrade accuracy. In contrast, applying t-SNE directly to time-frequency representations yields the best performance. Specifically, the combination of CWT and t-SNE achieves a classification accuracy of 99.69% with KNN and 99.61% with SVM. These findings indicate that dimensionality reduction applied directly to time-frequency representations can preserve discriminative information and improve bearing fault classification compared with conventional feature extraction strategies. The findings further indicate that combining suitable signal representations with dimensionality reduction can enable conventional classifiers to deliver strong diagnostic performance.

1. Introduction

Rotating machinery relies heavily on rolling bearings, but they are highly prone to failure under harsh operating conditions such as high loads and variable speeds [1]. Faults affecting the inner race, outer race, rolling elements, and cage represent approximately 40–45% of rotating machinery failures [2]. Therefore, developing effective diagnostic and condition-monitoring methods is crucial to prevent economic losses and ensure system safety. In Industry 4.0, vibration analysis is widely used for predictive maintenance, particularly for bearing fault diagnosis. Vibration signals provide useful data for assessing the condition of the system.

Numerous studies have proposed different preprocessing strategies. However, most existing approaches rely on conventional pipelines in which a single preprocessing stage is followed by feature extraction. Dimensionality reduction is sometimes applied subsequently to the extracted features.

In [3], the authors propose a fault diagnosis methodology that extracts and fuses time-frequency and acoustic features. The extracted features are subsequently processed through Principal Component Analysis (PCA) to obtain a reduced representation before classification.

In [4], the authors employ signal filtering and segmentation before transforming the signals into time-frequency maps through the Continuous Wavelet Transform (CWT). Their approach performs classification without an explicit dimensionality reduction step.

In [5], the authors transform vibration signals into time-frequency representations using CWT. Convolutional Neural Networks (CNNs) subsequently perform feature extraction and classification without an intermediate dimensionality reduction step.

In [6], the authors use the CWT to convert one-dimensional vibration data into two-dimensional time-frequency maps for identifying bearing faults.

In [7], the authors use the Short-Time Fourier Transform (STFT) to generate time-frequency images. An attention-based CNN then processes these images, with pooling operations implicitly performing dimensionality reduction.

In [8], the authors propose a bearing fault diagnosis method that combines STFT with six time-domain statistical features. An attention-based fusion module integrates these features, and PCA reduces redundancy and helps prevent overfitting. The authors also employ an adaptive Lévy-seagull optimization algorithm to improve diagnostic accuracy and model efficiency.

In [9], the authors propose an explainable artificial intelligence (AI)-based approach for bearing fault diagnosis. They use STFT to generate spectrograms and Gradient-weighted Class Activation Mapping (Grad-CAM) to highlight relevant features. The approach aims to improve diagnostic accuracy and interpretability while supporting outlier detection.

In [2], the authors propose a hybrid approach that combines the Hilbert Transform and the Fast Kurtogram (FK) with signal decomposition techniques and envelope analysis. Their approach mainly relies on handcrafted indicators.

Similarly, the authors of [10] propose a method called HTMFK, which combines the Hilbert Transform with a modified FK. The method aims to improve resonance frequency band identification and fault detection under noisy and variable-speed conditions.

In [11], the authors introduce a variant of the Kurtogram that incorporates Wavelet Packet Decomposition (WPD) as a filter to address some limitations of the original method.

In studies [12-14], researchers use t-distributed Stochastic Neighbor Embedding (t-SNE) to reduce feature dimensionality for bearing fault diagnosis. This method maps high-dimensional features into a lower-dimensional space while preserving local relationships, thereby facilitating feature analysis and subsequent processing using machine learning algorithms.

In [15], the authors apply t-SNE to visualize and identify multiple planetary gearbox faults using vibration-based features. They compare its performance with that of Stochastic Neighbor Embedding (SNE) and PCA. Their results indicate that t-SNE provides better fault visualization and separation.

In [16], the authors propose a lightweight transfer learning framework for high-speed railway bearings, addressing fault diagnosis when labeled samples are scarce and multiple faults are present. They evaluate domain adaptation using t-SNE visualization, which demonstrates alignment between the source and target feature distributions.

In [17], the authors combine an improved composite multi-scale fuzzy entropy method with t-SNE for feature dimensionality reduction. They use the Beetle Antennae Search (BAS) algorithm to optimize Support Vector Machine (SVM) parameters.

Similarly, the authors of [18] combine t-SNE with the Whale Optimization Algorithm (WOA) to optimize SVM parameters for bearing fault diagnosis.

In [19], the authors use t-SNE to visualize entropy features extracted using five measures. They assess inter-class separability and intra-class compactness based on the resulting visualization. Combined with K-Nearest Neighbors (KNN), the method achieves nearly perfect classification accuracy and outperforms the Backpropagation Neural Network (BPNN).
Overall, these studies show that traditional methodologies focus on feature extraction after preprocessing, while the direct exploitation of time-frequency representations through dedicated dimensionality reduction techniques remains limited. This observation motivates the approach proposed in this study.
In particular, this work evaluates the performance of raw and preprocessed signals using FK, STFT, and CWT. Furthermore, t-SNE is applied directly to the time-frequency matrices to preserve their intrinsic structure.
Simple classification algorithms, namely SVM and KNN, are adopted to ensure that the evaluation focuses on the effectiveness of the signal processing strategy rather than on model complexity.

2. Signal processing techniques

This study employs the FK, STFT, and CWT to compare their ability to enhance fault-related transients and extract discriminative features under identical conditions. This comparison aims to identify the most appropriate method for bearing fault diagnosis.

2.1. Fast kurtogram

The Fast Kurtogram is an efficient implementation of the Kurtogram developed to rapidly identify the frequency band exhibiting the highest Spectral Kurtosis (SK). Kurtosis measures the impulsiveness of a signal, which is closely related to faults in rotating machinery.
SK extends this concept by evaluating how impulsiveness varies across frequency bands, allowing the detection of modulated transients associated with bearing defects. By computing kurtosis across different frequency bands, FK localizes fault-related non-stationary components in the frequency domain [20].

The authors of [21] introduced FK as a fast algorithm for computing the Kurtogram. Fig. 1 represents an FK image, showing SK values across different frequency bands in the frequency domain. Each colored block corresponds to a frequency band, highlighting regions with high impulsiveness.

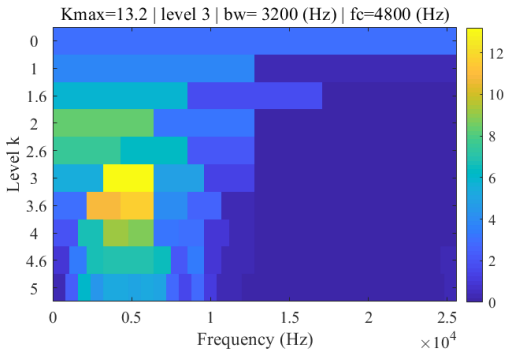

Fig. 1. Sample of the FK.

Each colored block represents a frequency band (Bw), where the color indicates the corresponding SK value. The block width represents the bandwidth, while its horizontal position corresponds to the center frequency (fc). The frequency band with the highest SK value defines the optimal band-pass filter parameters.

2.2. Short-time Fourier transform

The Short-Time Fourier Transform is widely used for the time-frequency analysis of non-stationary signals. It transforms one-dimensional vibration signals into two-dimensional representations containing both time and frequency information [22].
Unlike the conventional Fourier transform, which provides only global frequency information, STFT captures the temporal evolution of the signal [23]. It applies a fixed-length window and computes the Fourier transform of each segment. This process produces a time-frequency representation, mathematically expressed in Eq. (1) [22]:

$$X(t) = \int_{-\infty}^{+\infty} \mathrm{x}(s).\,\mathrm{g}(s-t).\,\mathrm{e}^{-j\omega t}\,\mathrm{d}s \qquad (1)$$

where x(t) is the time-domain signal; t and s denote time; w denotes the frequency; and g(s −

t) is a window function whose center is at time t.
STFT analyzes signal variations over time by generating a time-frequency representation that describes changes in frequency content. This representation captures signal characteristics at different time and frequency locations, making STFT suitable for non-stationary signal analysis [23].
In vibration analysis, STFT is widely used for fault diagnosis because it reveals time-varying frequency characteristics. These characteristics facilitate fault identification and condition monitoring [23].
In this study, STFT was computed using a Hamming window to reduce spectral leakage and improve the reliability of the spectral representation.
The window length was determined using five periods of the minimum frequency of interest. This choice provides a compromise between time and frequency resolution. A 50% overlap was adopted to reduce information loss between consecutive frames and produce a smoother time-frequency representation.
The Fast Fourier Transform (FFT) size was set to the length of the input signal to obtain a detailed frequency-domain representation. These settings support the analysis of transient and frequency-dependent characteristics in bearing vibration signals.

2.3. Continuous wavelet transforms

The Continuous Wavelet Transform is a time-frequency analysis technique widely used for non-stationary signals with time-varying frequency components. It converts a signal from the time domain into the time-frequency domain by applying wavelets at different scales and positions, producing coefficients that describe the signal's frequency behavior over time [24].
The mathematical expression of CWT is given in Eq. (2) [24]:

$$C(a,b) = \int_{-\infty}^{+\infty} x(t).\psi_{a,b}^{*}(t)\,dt \qquad (2)$$

where x(t) represents the vibrational signal; $\psi a,b$ (t) represents the wavelet function with scale a and position offset b (Stretched and translated version of the parent wavelet); ψ^* is the complex conjugate of ψ; C(a, b) is the CWT coefficient that represents the amplitude and phase of a frequency associated with a at time b.
In this study, CWT was computed using the analytic Morlet wavelet, which is suitable for analyzing oscillatory components and transient features in vibration signals. The number of voices per octave was set to 48 to provide fine frequency resolution across the analyzed frequency range.
The frequency limits were set to [50–4000] Hz to focus the analysis on the frequency components of interest. Absolute values of the wavelet coefficients were retained to represent the magnitude of the time-frequency components and facilitate the identification of fault-related patterns.
Finally, 50 frequency values were selected to obtain a compact time-frequency representation for subsequent analysis.

3. Methodology and diagnostic approach

This study evaluates the contribution of signal processing to bearing fault diagnosis by investigating its integration with feature extraction and dimensionality reduction. To validate the proposed strategy, simple classifiers, namely SVM and KNN, are used instead of complex models.
First, the contribution of signal preprocessing is assessed by comparing raw and preprocessed vibration signals. Specifically, a baseline using raw signals is compared with a framework that applies FK, STFT, and CWT before feature extraction and classification. This analysis evaluates the effect of preprocessing on feature quality and diagnostic performance.
Second, the effect of applying t-SNE directly to the STFT and CWT time-frequency matrices is examined and compared with the results obtained after features extraction. This comparison determines whether direct dimensionality reduction of time-frequency representations improves signal representation and classification accuracy.
Overall, this methodology provides a structured evaluation of how each processing stage influences fault diagnosis performance. The

contributions of raw signals, preprocessing techniques, and dimensionality reduction applied directly to time-frequency representations are systematically compared.
This approach also enables the evaluation of strategies for enhancing fault-related information while maintaining a simple and efficient diagnostic framework based on SVM and KNN.
Furthermore, the Polar Lights Optimizer (PLO) is used to optimize the hyperparameters of SVM and KNN. This optimization enables a systematic comparison of the two analysis strategies under optimized classification settings.

3.1. Feature extraction

Feature extraction is a fundamental step in degradation assessment because vibration signals contain valuable information about bearing health. Among the commonly used time-domain indicators, Root Mean Square (RMS) and kurtosis are widely adopted to characterize signal variations [25].
This study uses a set of time-domain indicators to characterize the vibration signals. These include the RMS, Skewness, Kurtosis, Standard Deviation (STD), Interquartile Range (IQR), Maximum value (MAX), Median Absolute Deviation, Peak-to-Peak value, Variance, and the 75th Percentile (P75).
These indicators were selected because they capture different statistical properties of the signal, such as dispersion, impulsiveness, and amplitude variations, which are essential for effectively describing bearing fault characteristics.

3.2. Applying t-distributed stochastic neighbor embedding

The t-distributed Stochastic Neighbor Embedding is a nonlinear dimensionality reduction technique that projects high-dimensional data into a low-dimensional space. It was derived from the SNE algorithm [26].
Compared with other dimensionality reduction methods, t-SNE provides superior visualization of high-dimensional data. It has been widely applied in medical analysis, biological research, and computer security [26].
The t-SNE algorithm measures similarity between high-dimensional samples by modeling their joint probability distribution. It then seeks a corresponding low-dimensional representation that preserves these similarities. The optimal embedding is obtained by minimizing the Kullback-Leibler (KL) divergence between the two probability distributions [26].

3.3. Machine learning-based diagnosis

SVM and KNN are used for bearing fault diagnosis because of their simplicity, robustness, and effectiveness. These classifiers allow the evaluation of signal processing and feature representation without introducing unnecessary model complexity.
The KNN algorithm is a straightforward and widely adopted classification method that predicts the class of a sample based on the majority class of its nearest neighbors in the feature space. Its effectiveness is influenced by the distance metric, the number of neighbors, and the decision rule, making it well suited for multi-class bearing fault diagnosis.
SVM is a machine learning algorithm derived from statistical learning theory and is widely applied to nonlinear and small-sample classification problems. It constructs an optimal separating hyperplane by maximizing the margin between classes, making it well suited for bearing fault diagnosis with limited training data.
The performance of the KNN and SVM classifiers is optimized using the PLO to identify the hyperparameters that maximize classification accuracy.
For KNN, four parameters are optimized: the number of neighbors (K), the distance metric (Euclidean, cityblock, cosine, and Chebyshev), the distance weighting scheme (equal, inverse, and squared inverse), and data standardization. These parameters influence similarity measurement in the feature space and the classifier's generalization capability.
For SVM, four parameters are optimized: the regularization parameter (C), the kernel scale (γ), the kernel function (linear, RBF, and

polynomial), and data standardization. These parameters improve the discriminative capability and robustness of the classifier for complex fault diagnosis tasks.

PLO was selected for its ability to balance global exploration and local exploitation. Unlike conventional metaheuristic algorithms such as Artificial Bee Colony (ABC) and Particle Swarm Optimization (PSO), PLO uses adaptive stochastic movements inspired by polar light dynamics to explore the search space and promote convergence.

PLO is designed to reduce the risk of premature convergence compared with PSO and to enhance exploration compared with ABC through its Gaussian-based perturbation mechanism. Moreover, PLO requires fewer control parameters, which simplifies its implementation and reduces the tuning effort. The characteristics make PLO particularly suitable for hyperparameter optimization in nonlinear and multimodal problems such as vibration-based fault diagnosis, where achieving both robustness and high classification accuracy is critical [27].

4. Dataset

The Hanoi University of Science and Technology (HUST) dataset [28], introduced by Thuan and Hong in 2023, is a benchmark dataset for ball bearing fault diagnosis. Bearing defects were artificially introduced using a wire-cut technique to produce a 0.2 mm microcrack, as illustrated in Fig. 2, to simulate early-stage faults. The vibration data were acquired from a motor operating under a low-load condition at a sampling frequency of 51.2 kHz. A notable characteristic of this dataset is the artificial introduction of bearing defects. The dataset also considers the mechanical interaction between defects, whereby one fault may contribute to the development of another.

The dataset comprises 98 raw vibration signals collected from five bearing types under three operating conditions. It covers six fault categories: inner crack, outer crack, ball crack, inner-outer cracks, inner-ball cracks, and outer-ball cracks.



Fig. 2. Representative bearing defects considered in the experimental study: (a) Inner-race defect; (b) Outer-race defect; (c) Rolling-element defect; (d) Inner-race and outer-race defects; (e) Inner-race and rolling-element defects; and (f) Outer-race and rolling-element defects. The corresponding defect locations are marked by red circles [28].

The number of signals varies across fault categories because of differences in data availability. For healthy bearings, inner cracks, outer cracks, and inner-outer cracks, signals are available for all five bearing types under three operating conditions, yielding 15 signals per category.

For ball cracks and inner-ball cracks, data are available for four bearing types under three operating conditions, yielding 12 signals per category. For outer-ball cracks, data cover two operating conditions for one bearing type and three operating conditions for each of the four remaining types, yielding 14 signals. Thus, the dataset contains 98 raw vibration signals in total ($4 \times 15 + 2 \times 12 + 14 = 98$).

5. Results and discussion

To evaluate the proposed method, experiments were conducted using the HUST bearing dataset [28], which covers six fault categories and the healthy condition (seven classes) across multiple bearing types and operating conditions, providing a diverse set of vibration signals for performance evaluation.

In the first stage, raw vibration signals were compared with signals processed using the FK, STFT, and CWT before feature extraction. To increase the number of samples, each of the 98 raw vibration signals was divided into 50 segments using simple segmentation, yielding 4900 samples in total.

Ten features were then extracted from each segment, with each feature providing 4900 values. Consequently, a final feature matrix of size [4900,10] was obtained for subsequent analysis and classification.

Fig. 3 illustrates RMS-based feature extraction from the raw vibration signal, while Fig. 4 shows

the corresponding extraction performed on the CWT coefficients. The RMS profiles derived from the raw signal and from the CWT coefficients exhibit variations across samples, reflecting changes in the signal content.
The comparison between the two figures also reveals differences in the magnitude of the RMS values.

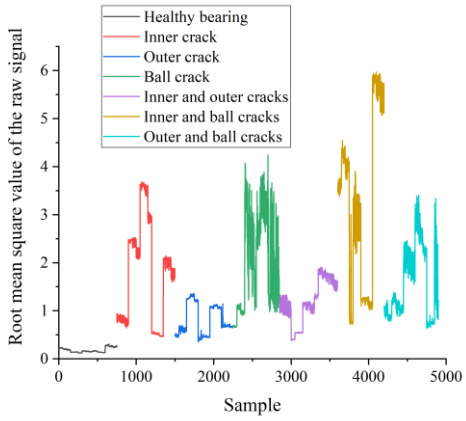

Fig. 3. RMS feature extraction from raw signal.

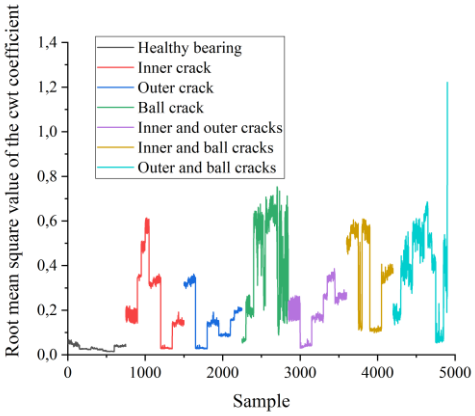

Fig. 4. RMS feature extraction from CWT coefficients.

The raw signal exhibits a wider range of RMS values, whereas the RMS values derived from the CWT coefficients remain within a lower range. This difference reflects the distinct characteristics of the two representations.
Whether the higher RMS magnitudes observed in the raw signals contribute to improved classification performance will be examined through the classification results presented in the following sections. However, the figure does not clearly reveal distinct or well-separated patterns that can be directly associated with specific fault conditions. The distributions appear relatively continuous, making it difficult to visually distinguish between different classes.
Therefore, although RMS and other time-domain indicators provide a compact representation of the signal, their discriminative capability cannot be conclusively assessed from this figure alone. Additional analysis or complementary techniques are required to better evaluate the separability of the extracted features.
In the second stage, t-SNE was applied directly to the time-frequency coefficient matrices obtained using CWT and STFT to compare the feature representations provided by the two methods.
For each of the 98 raw vibration signals, both methods generated a coefficient matrix of size [50,10], where 50 represents the number of selected frequency components, and M is the input signal length.
The value of 50 was selected as a compromise between retaining sufficient information from the time-frequency representation and maintaining a reasonable computational cost.
Using fewer frequency components could result in the loss of relevant information, whereas using substantially more components would increase the computational cost and produce a larger representation than necessary. Therefore, 50 frequency components were retained for each CWT and STFT representation.
The t-SNE algorithm was then applied to each coefficient matrix to produce a 10-dimensional feature representation, yielding a reduced feature matrix of size [50,10] per signal. By processing all 98 signals, a final feature matrix of size [4900,10] was obtained for each method, enabling a direct comparison of CWT- and STFT-based representations.
Fig. 5 illustrates the t-SNE-based feature extraction procedure, in which high-dimensional samples are mapped to a lower-dimensional space.
The first t-SNE dimension exhibits different value ranges and fluctuation patterns across the seven bearing conditions. Some classes show

pronounced variations, whereas others display more localized values.

The projection shows that the transformed samples are separated into multiple clusters within the low-dimensional space.

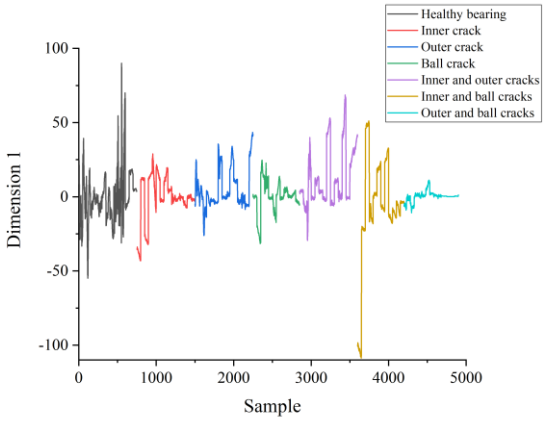

Fig. 5. Feature extraction using t-SNE.

Some regions appear more concentrated, suggesting local similarity between samples, while other regions show a more dispersed distribution. However, the boundaries between groups are not strictly defined, and certain overlaps may be present.

These observations indicate that t-SNE reveals an underlying structure in the data, but the degree of class separability cannot be definitively concluded without additional labeling or quantitative evaluation. The figure mainly provides a qualitative insight into the organization of the data rather than a definitive assessment of classification performance.

No superiority of either approach is assumed. Instead, the two figures provide complementary perspectives: RMS summarizes the signal characteristics, while t-SNE enables a qualitative visualization of the relationships between the coefficients of the time-frequency matrix.

The holdout validation strategy was used to evaluate the proposed approach for seven-class classification, comprising one healthy condition and six fault categories. The healthy condition was included as an essential reference class to enable the identification of normal bearing operation and its distinction from the six fault conditions.

The 4900 samples were randomly partitioned into training and testing sets, with 70% (3430 samples) allocated to training and the remaining 30% (1470 samples) reserved for testing. This partitioning ensured that all seven classes were represented in both subsets.

As described in the methodology section, the SVM and KNN classifiers were used for bearing fault classification, with their hyperparameters optimized using the PLO.

The performance of each model was assessed over 10 independent experimental runs using classification accuracy (ACC). The minimum, maximum, mean, and STD of ACC were calculated to evaluate both the classification performance and the stability of the models.

Table 1 presents the classification results obtained using feature extraction applied to raw and preprocessed signals.

Fig. 6 illustrates the distribution of classification accuracy obtained over 10 experimental runs using SVM and KNN with raw signals and the FK, STFT, and CWT preprocessing methods. The box plots also provide information about the variability of classification accuracy across the experimental runs.

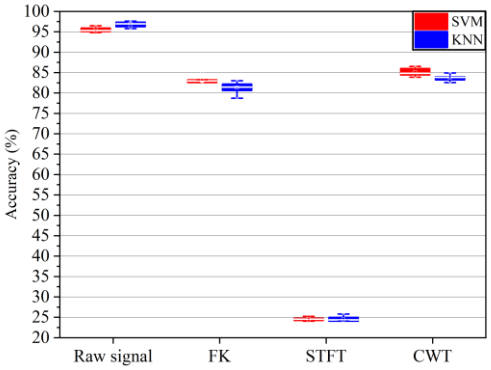

Fig. 6. Evaluation of classification ACC using feature extraction from raw and preprocessed signals.

The baseline results obtained using raw signals show high classification performance, with mean ACC of 95.35% for SVM and 96.83% for KNN, indicating that the extracted features already contain relevant discriminative information.

Table 1. Performance using feature extraction.

Pretreatment	AI classifier	Min ACC [%]	Max ACC [%]	STD ACC	Mean ACC [%]
Raw signal	SVM	93.53	96.46	0.84	95.35
	KNN	95.78	97.61	0.60	96.83
FK	SVM	82.58	84.62	0.60	83.05
	KNN	78.70	82.99	1.21	81.31
STFT	SVM	22.44	25.71	0.85	24.44
	KNN	22.72	25.78	0.83	24.46
CWT	SVM	83.87	86.53	0.89	85.05
	KNN	82.58	84.89	0.69	83.75

However, when preprocessing techniques are introduced, classification performance varies depending on the method. The FK reduces the ACC of both classifiers, particularly KNN, suggesting that the preprocessing stage may not preserve all relevant information required for effective classification.

The STFT-based approach exhibits very poor classification performance, with a mean ACC of approximately 24% for both classifiers. These results suggest that feature extraction from STFT representations does not provide sufficiently discriminative information for effective bearing fault classification under the considered configuration.

In contrast, the CWT-based approach achieves relatively high classification ACC (approximately 85%), demonstrating its ability to provide a more suitable representation of non-stationary and transient signal characteristics than STFT.

Overall, the raw signal outperforms most preprocessing-based approaches. This indicates that preprocessing may reduce diagnostic performance when not adapted to signal characteristics. Therefore, preprocessing is not always beneficial and must be carefully designed, as inappropriate processing may cause the loss of relevant information.

Table 2 reports the results obtained when dimensionality reduction is applied directly to the STFT and CWT matrices using t-SNE, instead of performing feature extraction. A significant improvement in performance can be observed compared to the results in Table 1.

Fig. 7 illustrates the distribution of classification ACC obtained over 10 experimental runs using SVM and KNN after applying t-SNE to the CWT and STFT coefficient matrices.

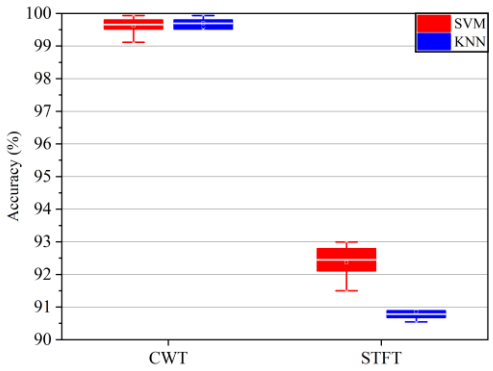

Fig. 7. Evaluation of classification ACC using t-SNE-based dimensionality reduction of CWT and STFT representations.

For STFT, the classification ACC increases considerably from approximately 24% to over 92% with SVM. This suggests that the low performance reported in Table 1 is related not only to the time-frequency representation itself but also to the feature extraction process applied to it.

These results indicate that preserving the information contained in the time-frequency coefficient matrix through dimensionality reduction can be more effective than relying on the extracted time-domain features in the considered configuration.

Table 2. Performance using t-SNE.

Pretreatment	AI classifier	Min ACC [%]	Max ACC [%]	STD ACC	Mean ACC [%]
STFT	SVM	91.49	92.99	0.52	92.36
	KNN	90.54	91.42	0.26	90.85
CWT	SVM	99.11	99.93	0.25	99.61
	KNN	99.52	99.93	0.14	99.69

The highest classification accuracies are obtained with the CWT + t-SNE combination, reaching 99.61% for SVM and 99.69% for KNN, with very low standard deviations. This indicates not only high accuracy but also strong stability and robustness of the proposed approach.

These findings clearly demonstrate that applying dimensionality reduction directly to time-frequency representations is significantly more effective than conventional feature extraction methods.

The proposed approach was compared with several recent state-of-the-art methods for bearing fault diagnosis. As reported in [29], the Adaptive Convolutional Network with Batch Normalization (ACN-BM) achieved a classification accuracy of 98.78%.

Similarly, the Multi-Scale Fuzzy Logic Classifier (MSFLZC) presented in [30] reached 98.91%, demonstrating the effectiveness of advanced intelligent diagnostic approaches.

In contrast, the hybrid deep learning framework in [31], combining a Wide Deep CNN, Bidirectional Long Short-Term Memory (BiLSTM), and a Spiking Neural Network (SNN), achieved a considerably lower accuracy of 83.11%, indicating that increased model complexity does not necessarily improve diagnostic performance.

The proposed method, which combines the CWT with t-SNE, achieved the highest classification performance among the compared methods.

Specifically, the KNN classifier obtained an ACC of 99.69%, while the SVM classifier achieved 99.61%, confirming the robustness and discriminative capability of the proposed feature representation.

These results demonstrate that directly applying dimensionality reduction to time-frequency representations effectively preserves the intrinsic structure of the vibration signals while improving class separability.

Overall, the findings indicate that an appropriate signal representation combined with an effective dimensionality reduction technique can outperform more sophisticated deep learning models, highlighting that the quality of feature representation has a greater impact on bearing fault diagnosis than the complexity of the classification algorithm.

6. Conclusions

The results obtained in this study provide valuable insights into the influence of signal processing techniques on bearing fault diagnosis. First, the raw signal demonstrates a strong capability to achieve high classification performance, indicating that it already contains sufficiently discriminative information for diagnosis. This finding suggests that baseline approaches should not be overlooked when evaluating advanced signal processing strategies.

Second, the results show that preprocessing techniques do not systematically improve performance and may even degrade the results if applied without careful consideration. This highlights the need to adapt preprocessing methods to signal characteristics and diagnostic requirements.

Third, the proposed approach, based on applying dimensionality reduction using t-SNE directly to time-frequency matrices, represents an effective and original strategy. Unlike traditional feature extraction methods, this approach preserves the intrinsic structure of the signal representation and leads to significantly improved classification performance, demonstrating better performance than the conventional techniques evaluated in this study.

Finally, the results confirm that an appropriate signal processing strategy can significantly enhance diagnostic performance even when

using simple classifiers such as SVM and KNN. This highlights that the effectiveness of the overall framework relies more on the quality of the signal representation than on the complexity of the classification model, offering a competitive alternative to more complex deep learning approaches.

References

[1] Q. Ni, J. C. Ji, K. Feng and B. Halkon, "A fault information-guided variational mode decomposition (FIVMD) method for rolling element bearings diagnosis", *Mech. Syst. Signal Process.*, Vol. 164, art. 108216, (2022).

[2] K. Bouaouiche, Y. Menasria and D. Khalfa, "Detection of defects in a bearing by analysis of vibration signals", *Diagnostyka*, Vol. 24, No. 2, art. 2023203, (2023).

[3] M. Sehri and P. Dumond, "Exploring Rolling Element Bearing Data Collection and Algorithm Hyperparameters for Machine Learning-Based Fault Diagnosis", *Int. J. Progn. Health Manag.*, Vol. 16, No. 2, art. 4372, (2025).

[4] T. Wang, C. Lu, Y. Sun, M. Yang, C. Liu and C. Ou, "Automatic ECG Classification Using Continuous Wavelet Transform and Convolutional Neural Network", *Entropy*, Vol. 23, No. 1, art. 119, (2021).

[5] H. Yu and H. Wei, "Lubrication state identification of vibration time-frequency characteristics based on CWT and CNN", *Sci. Rep.*, Vol. 15, No. 1, art. 28936, (2025).

[6] R. Boudiaf, B. Abdelkarim and H. Issam, "Bearing fault diagnosis in induction motor using continuous wavelet transform and convolutional neural networks", *Int. J. Electr. Comput. Eng.*, Vol. 15, No. 1, pp. 591–602, (2024).

[7] S. Yan, H. Wei, C. Yang, Z. Liu, S. Zhang and L. Zhao, "Fault Diagnosis of Rolling Bearing Based on CBAM-ICNN", *in 2024 39th Youth Academic Annual Conference of Chinese Association of Automation (YAC), Dalian, China: IEEE.*, pp. 1420–1425, (2024).

[8] H. Bai, W. Tong, C. Duan, Y. Zhou and S. Dong, "Rolling bearing fault diagnosis method based on fusion of STFT-statistical features and AL-SOA optimized bagging tree", *Sci. Rep.*, Vol. 16, No. 1, art. 10314, (2026).

[9] K. Kim and Y. S. Kim, "Vibration spectrogram analysis for bearing fault diagnosis based on grad-cam for feature selection and statistical approach", *J. Mech. Sci. Technol.*, Vol. 38, No. 11, pp. 5885–5898, (2024).

[10] C. Yue, Y. Zhu, P. Cheng, B. Wang and K. Wang, "A novel method for identifying resonance frequency band in weak bearing fault diagnosis of electric driving system", *Shock Vib.*, Vol. 2024, art. 2804173, (2024).

[11] Y. Lei, J. Lin, Z. He and Y. Zi, "Application of an improved kurtogram method for fault diagnosis of rolling element bearings", *Mech. Syst. Signal Process.*, Vol. 25, No. 5, pp. 1738–1749, (2011).

[12] A. Jabbar, M. Cocconcelli and G. D'Elia, "Intelligent time–frequency feature embedding and reshaping for bearing fault diagnosis in motion control applications", *Mech. Syst. Signal Process.*, Vol. 250, art. 114191, (2026).

[13] D. Tu, J. Zheng, Z. Jiang and H. Pan, "Multiscale distribution entropy and t-distributed stochastic neighbor embedding-based fault diagnosis of rolling bearings", *Entropy*, Vol. 20, No. 5, art. 360, (2018).

[14] J. Chen, D. Zhou, C. Lyu and C. Lu, "Feature reconstruction based on t-SNE: an approach for fault diagnosis of rotating machinery", *J. Vibroeng.*, Vol. 19, No. 7, pp. 5047–5060, (2017).

[15] J. Chen, C. Wang, B. Wang and Z. Zhou, "A visualized classification method via t-distributed stochastic neighbor embedding and various diagnostic parameters for planetary gearbox fault identification from raw mechanical data", *Sens. Actuators A Phys.*, Vol. 284, pp. 52–65, (2018).

[16] H. Zheng et al., "Dirichlet-weighted composite data synthesis for robust transfer learning in high-speed railway bearing fault diagnosis", *PeerJ Comput. Sci.*, Vol. 12, art. e4075, (2026).

[17] S. Wang, C. Wang, Y. Lian and B. Luo, "Research on bearing fault diagnosis based on VMD-RCMWPE feature extraction and WOA-SVM-optimized multidataset fusion", *Sensors*, Vol. 25, No. 16, art. 5139, (2025).

[18] B. Wu, Z. Wang and X. Ye, "Rolling bearing fault diagnosis based on ICMFE, t-SNE, and BAS-SVM", *Meas. Control*, Vol. 59, No. 5, pp. 709–725, (2026).

[19] Y. Li, J. Yue and S. Chen, "Two-dimensional pattern entropy for bearing fault diagnosis", *Chaos Solitons Fractals*, Vol. 209, art. 118558, (2026).

[20] A. Afia, C. Rahmoune and D. Benazzouz, "Gear fault diagnosis using Autogram analysis", *Adv.*

Mech. Eng., Vol. 10, No. 12, art. 168781401881253, (2018).
[21] J. Antoni, "Fast computation of the kurtogram for the detection of transient faults", *Mech. Syst. Signal Process.*, Vol. 21, No. 1, pp. 108–124, (2007).
[22] H. Tao, P. Wang, Y. Chen, V. Stojanovic and H. Yang, "An unsupervised fault diagnosis method for rolling bearing using STFT and generative neural networks", *J. Franklin Inst.*, Vol. 357, No. 11, pp. 7286–7307, (2020).
[23] H. Huang, Y. Hou, Z. Chen, Y. Han and X. Zhai, "Fault diagnosis model based on STFT and multi-scale convolution channel attention", *in 2025 IEEE 14th Data Driven Control and Learning Systems (DDCLS), Wuxi, China: IEEE.* , pp. 1576–1581, (2025).
[24] J. Du, X. Li, Y. Gao and L. Gao, "Integrated Gradient-Based Continuous Wavelet Transform for Bearing Fault Diagnosis", *Sensors*, Vol. 22, No. 22, art. 8760, (2022).
[25] B. Zhang, S. Zhang and W. Li, "Bearing performance degradation assessment using long short-term memory recurrent network", *Comput. Ind.*, Vol. 106, pp. 14–29, (2019).
[26] J. Liu, Q. Li, H. Yang, Y. Han, S. Jiang and W. Chen, "Sequence Fault Diagnosis for PEMFC Water Management Subsystem Using Deep Learning With t-SNE", *IEEE Access*, Vol. 7, pp. 92009–92019, (2019).
[27] Z. A. Almishlih, O. S. Qasim and Z. Y. Algamal, "Design and evaluation of a new tent-shaped transfer function using the Polar Lights Optimizer algorithm for feature selection", *IAPGOS*, Vol. 15, No. 2, pp. 27–31, (2025).
[28] N. D. Thuan and H. S. Hong, "HUST bearing: a practical dataset for ball bearing fault diagnosis", *BMC Res. Notes*, Vol. 16, No. 1, art. 138, (2023).
[29] P. Hou, J. Zhang, Z. Jiang, Y. Tang and Y. Lin, "A Bearing Fault Diagnosis Method Based on Dilated Convolution and Multi-Head Self-Attention Mechanism", *Appl. Sci.*, Vol. 13, No. 23, art. 12770, (2023).
[30] Y. Li, J. Yue and Y. Zhao, "Multiscale Similarity Fuzzy Lempel-Ziv Complexity and Its Application in Bearing Fault Diagnosis", *IEEE Trans. Instrum. Meas.*, Vol. 75, pp. 1–13, (2026).
[31] C. Bian, C. Jia, J. Li, X. Chen and P. Wang, "Rolling bearing fault diagnosis under small sample conditions based on WDCNN-BiLSTM Siamese network", *Sci. Rep.*, Vol. 15, No. 1, art. 29591, (2025).